J. Fluid Mech. (1980), *vol.* 97, *part* 1, *pp.* 65–89
Printed in Great Britain

Turbulence measurements in a constricted tube

By M. D. DESHPANDE

Department of Mechanical Engineering, The Catholic University of America, Washington, D.C. 20064

AND D. P. GIDDENS

School of Aerospace Engineering, Georgia Institute of Technology, Atlanta, Georgia 30332

(Received 17 May 1978 and in revised form 5 March 1979)

Measurements of turbulent flow through a constricted tube with a contoured 75 % constriction have been performed with a laser-Doppler anemometer. One motivation for these studies was the problem of flow through arterial stenoses and consequently a range of relatively low Reynolds numbers (5000–15000) was employed. Velocity profiles, r.m.s. turbulence velocities, and energy spectra were recorded along with determinations of the wall pressure variation and length of recirculation region. Results show extremely high levels of turbulence and considerable turmoil within the so-called recirculation region. A method for determining the reattachment point in an intensely turbulent flow is given which should offer improvement over flow visualization techniques. Similarity in turbulence energy spectra measured at various radial positions is found at several axial locations, but does not occur in the region immediately downstream of separation. The downstream recovery of the turbulence velocity to upstream values takes place slowly. A secondary motivation of providing experimental data useful in evaluating turbulence models for computational fluid dynamics led to extensive measurements of radial and axial r.m.s. turbulence velocity components at a Reynolds number of 15000.

1. Introduction

The present study was motivated primarily by an interest in the fluid dynamics associated with subtotal constrictions, or stenoses, frequently encountered in atherosclerotic arteries. Theoretical work for steady laminar flow has been reported previously by Deshpande, Giddens & Mabon (1976) and results were compared with experimental data available in the literature. This paper reports on experimental studies of turbulent flow.

The possibility of disordered and turbulent flows occurring in the cardiovascular system is now accepted. It has been confirmed for normal vessels in animals, under certain conditions, by Seed & Wood (1971) and by Nerem & Seed (1972). Giddens, Mabon & Cassanova (1976) and Khalifa & Giddens (1978) have demonstrated that mild stenoses in the dog aorta create notable flow disorder and that portions of the turbulent field, distal to severe stenoses, are quasi-steady in behaviour over the Reynolds-number range studied. Stein & Sabbah (1976) used a hot-film anemometer probe to record velocity fluctuations in the ascending aorta of human subjects. In

0022-1120/80/4387-8370 $02.00

each of the eight patients having aortic valvular disease or a prosthetic aortic valve, turbulent flow occurred during systole.

Although the actual arterial stenosis may be of irregular geometry, it has been frequently modelled by the configuration of a constriction in a long tube. Examples of this are the works of Young & Tsai (1973), who studied the onset of poststenotic instabilities at low Reynolds number, and of Clark (1976), who employed several symmetrical and non-symmetrical nozzles to model stenosed aortic valves. Related subjects are the situations of a sudden enlargement in a pipe or a planar duct and of flow over a rearward-facing step. Roschke & Back (1976) report reattachment lengths measured in an abrupt expansion in a tube. Teyssandier & Wilson (1974) employ an integral approach to describe the sudden pipe enlargement problem and compare their analysis with the experimental data of Chaturvedi (1963). Durst, Melling & Whitelaw (1974) considered low-Reynolds-number flow through a sudden expansion. Their measurements were made in a plane duct to facilitate use of the laser-Doppler anemometer. A later study of Cherdron, Durst & Whitelaw (1978) extended this to a more thorough probing of asymmetries in the flow. By removing the upper wall of the planar duct, one obtains the geometry of flow over a rearward-facing step. Etheridge & Kemp (1978) performed laser-Doppler anemometer studies of turbulent flow in the separated region, and its vicinity, formed downstream of the step. Each of these laser studies present velocity profiles and turbulent velocity fluctuation data in the region of separated flow and concentrate on post-separation phenomena such as shear-layer development, turbulence within the 'separation bubble', and flow reattachment. The planar duct, however, is not a particularly good model for arterial flows since the confinement effects and non-symmetries (Cherdron *et al.* 1978) are rather different from the circular pipe case.

Since a localized pipe constriction or an enlargement creates a recirculation zone, these configurations have relevance to the problem of flow separation. The conditions prior to separation will, of course, have an effect on the distal region (Simpson, Strickland & Barr 1977; Hussain & Zedan 1978; Roshke & Back 1976). However, treatment of flow separation *per se* is complex and the constricted pipe geometry is not the best vehicle for an attack on this problem. Therefore, we (and others referenced here) have taken the approach of selecting a particular, well-defined geometry within which we explore the post stenotic flow field and have not studied the specific problem of boundary-layer separation.

We briefly mention a secondary motivation in performing this study. Without producing a list taken from the many available references, we point out that there is great interest in modelling turbulence for the purpose of computing turbulent flow fields. The situation of turbulent flow accelerating through a pipe convergence, separating under the influence of an adverse pressure gradient, undergoing intense turbulent fluctuations, reattaching, and eventually returning to a condition of fully developed pipe flow presents a tremendous challenge to the theoretician. A detailed set of experimental data for such a flow might be useful in testing, and perhaps refining, turbulence models.

To recapitulate, flow through vascular stenoses has an analogy in flow through constricted tubes. Very few experiments have been reported which give details of these fields; and most, though not all, data have been collected with hot-film or -wire instrumentation which suffers from inaccuracies in regions of separation, large flow

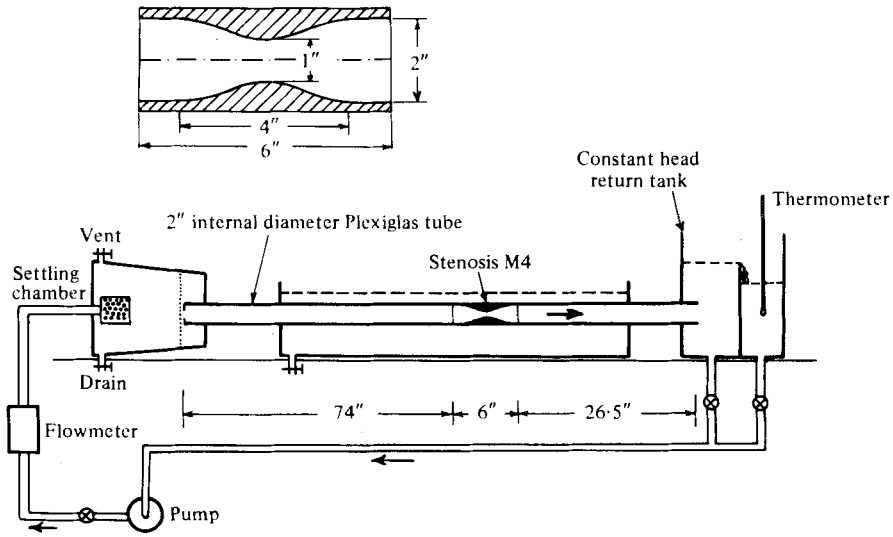

FIGURE 1. Schematic diagram of the flow system and the geometry of the stenosis model. Note: the axis of the laser is perpendicular to the plane of the paper.

angularities, and reversing velocities. Furthermore, *in vivo* data from Stein & Sabbah and Giddens *et al.* demonstrate that turbulent flow, distal to stenoses, exists during parts of the heart cycle. Therefore, in the spirit of attacking a complex problem from some tractable position, we have chosen to study initially the case of steady turbulent flow through a constriction. We aim at a twofold goal: first, to gain insight into phenomena occurring in the region of stenoses in large arteries; secondly, to provide a well-documented set of experimental data with which turbulent flow calculations may be compared. Our hope is that the results will thus be of interest to the general field of fluid dynamics as well as to that subset engaged in biomechanics studies.

We have therefore selected a 75 %, smoothly contoured constriction. This degree of area reduction should create an intensely turbulent field; and, in addition, it is well known that vascular stenoses less severe than this are usually haemodynamically insignificant (that is, there are virtually no presenting clinical symptoms of insufficiency of blood supply). Furthermore, the contoured occlusion, although not a precise model for arterial stenoses, is a more reasonable shape than an orifice. In addition, since it is hoped that the results may be of interest to computational fluid-dynamicists, the cosine shape selected is a well-defined one for theoretical studies (Smith 1976).

Experiments were performed at Reynolds numbers between 5000 and 15000 based upon conditions in the unoccluded portion of the tube. The lower values are of more interest from the biofluid dynamics standpoint while the higher values are likely to be of greater interest to those engaged in turbulence modelling.

2. Experimental arrangement

Flow system

Figure 1 illustrates the flow system and the geometry of the stenosis. Water was supplied by two centrifugal pumps to an upstream reservoir which fed the test section. A screen in this reservoir and a sharp-edged tripping ring placed at the entrance of the

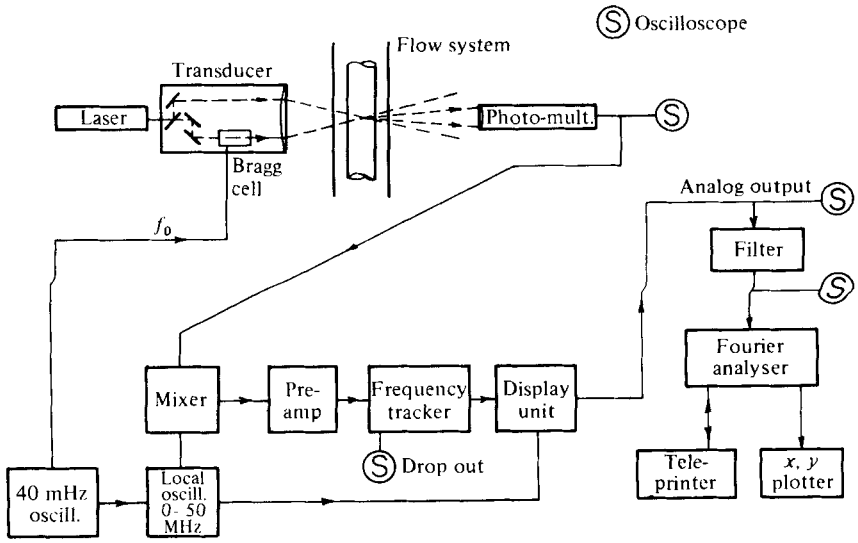

FIGURE 2. Block diagram of the LDA and Fourier analyser system.

2 in. (5·08 cm) inside-diameter Plexiglas tube assisted in the rapid development of a turbulent pipe flow. The stenosis was located 75 in. (190 cm) from the inlet and the length of tube distal to this constriction was 27·5 in. (70 cm). The pipe terminated in a constant-head tank and flow was regulated by valves in the return lines. Rotameter-type flowmeters were used to set the desired flow rate. The stenosis was machined and polished from a solid Plexiglas rod, using the contour

$$R_0(Z) = r_0(Z)/a_0 = 1 - \tfrac{1}{4}[1 + \cos \tfrac{1}{2}\pi Z] \quad (-2 \leqslant Z \leqslant 2),$$
$$= 1 \quad (|Z| > 2),$$

where a_0 is the unoccluded tube radius and r and z are the radial and axial co-ordinates which, when non-dimensionalized by a_0, form the dimensionless variables R and Z. The throat radius $R_0(0) = \frac{1}{2}$ corresponds to a 75 % reduction in cross-sectional area. Machining of the stenosis employed a template, and accuracy in adhering to the cosine shape was within 0·001 in. This contour was selected because it has been employed previously in theoretical calculations (Lee & Fung 1970;† Deshpande *et al.* 1976; Smith 1976) and because it provides a smooth constriction whose geometry is a fairly reasonable representation of an arterial stenosis.

A water-filled tank with flat Plexiglas walls surrounded the test section to reduce the effect of light refraction at the curved walls of the tube.

Instrumentation

The velocity measurements were taken with a DISA Model 55L Mark II laser-Doppler anemometer (LDA) employing the forward scatter mode (figure 2). A 5 mW helium–neon laser (wavelength 632·8 nm) provided the coherent light source. This beam was split in an optical package and one of the beams passed through a Bragg cell, creating a 40 MHz shift. The resulting pair of beams was then passed through a 12 cm focal length lens at beam separation distance of 4 cm. The resulting beam inter-section

† Lee & Fung (1970) used a Gaussian shape which closely resembles the cosine curve.

semi-angle, i_0, is 9·46° in air and yields a measuring volume approximating an ellipsoid of 0·12 mm width and 0·72 mm length. Because of differences in indices of refraction, the sampling volume in water is approximately 0·12 mm by 0·96 mm. Slight seeding was provided with silicon carbide particles of 1·5 μm average diameter. A 0·10 mm pinhole was set before the photomultiplier which detected the scattered light. The advantage of the Bragg cell is that the beam intersection contains a moving, rather than stationary, fringe pattern which allows the measurement of both forward and reverse velocities.

The signal processor is a phase-lock loop tracker and is described in a DISA publication.† Briefly, the frequency-modulated Doppler signal is compared with the output of a voltage-controlled oscillator (VCO) in such a manner as to maintain a constant phase relationship. The output of the VCO is then a measure of the Doppler frequency, including a d.c. offset created by the Bragg cell. The frequency-modulated Doppler signal is not ideal, however, owing to factors such as particle transit time, mean velocity gradients across the sample volume, turbulent velocity fluctuations within this volume, and electronic noise (see for example George & Lumley 1973). The effect of these is to create spectral broadening of the Doppler frequency and thus a measurement ambiguity which limits the response of the instrument to velocity fluctuations. Despite these limitations, very useful turbulence measurements may be obtained with the LDA. In our laboratory we have made repeated comparisons of the LDA and hot-film anemometer over a wide range of Reynolds numbers. Turbulence energy spectra (more precisely, the spectra of the square of a turbulence velocity component) show good agreement until frequencies are reached at which ambiguity becomes significant. Figure 3 gives an example of an LDA spectrum and compares this with the hot-film measurements of Resch (1970) in a fully developed turbulent pipe flow at $Re = 6100$.

Integration of the energy spectrum to form an r.m.s. turbulence velocity is a much more subtle proposition since, in principle, the integration must extend to infinite frequency. However, because the integral of the spectrum is bounded, truncation of the integration at some finite frequency value is appropriate owing to the very rapid roll-off of the spectrum as frequency increases. In calculating r.m.s. disturbance velocities for the flow ranges and optical configuration employed in the present study, a truncation of the integration at approximately 500 Hz gave results which had maximum estimated error on the order of 10 %. The appendix gives a discussion of estimation of error due to Doppler ambiguity and to truncation of the spectrum.

The laser and the optical package were mounted on an optical table and could be moved in two perpendicular directions in the horizontal plane and rotated about a vertical axis. All measurements were made in the plane of maximum tube diameter, passing horizontally through the tube axis. To measure the axial velocity V_z at any given position the two beams were kept in a horizontal plane while, for detection of the azimuthal velocity V_Φ, the beams were rotated into a vertical plane. Radial velocity was not measured owing to difficulties in accurately translating the laser and optics vertically with the apparatus available.

When the beams enter the water-filled tank surrounding the test section, the included angle reduces from $2i_0$ to $2i$, where $\sin i_0 / \sin i = \mu_w$, the index of refraction of water.

† DISA Type 55L Laser-Doppler Anemometer Mark II, Instruction Manual, DISA Electronics, Franklin Lakes, N.J. 07417 (1975).

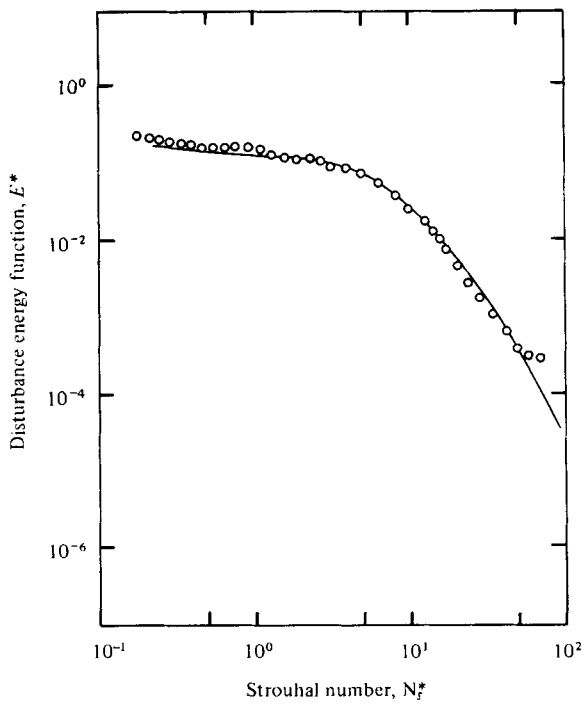

FIGURE 3. Turbulence energy spectrum measured with laser-Doppler anemometer (○) compared with hot-film measurements (——) of Resch (1970). Reynolds number is 6100.

Further, refractions take place owing to the curved wall of the tube and to the variable-thickness geometry of the stenosis. Corrections must account for

(i) changes in the beam intersection angle $2i$, and

(ii) the displacement of the measuring volume in the radial direction for V_Φ measurements and in both axial and radial directions for V_z measurements.

Changes in the direction of the bisector of the beam intersection angle are small in the case of V_z measurements and are neglected. The axial displacement in (ii) was accounted for while making measurements at various radial stations so that velocity profiles were always measured in a fixed plane perpendicular to the tube axis. These corrections were checked by moving the measurement volume from wall to wall and comparing the predicted and actual translational displacements of the laser. A further check results when the measured velocity profiles were found to be symmetric after optical corrections were applied. (The raw data are not symmetric and the corrections are unequal on either side of the axis.) Thorough discussion and derivation of the appropriate equations are given by Deshpande (1977).

The flow rate was kept constant while measuring the velocity profiles at a given station. The maximum change in temperature permitted in the downstream reservoir during this time was $\pm 0{\cdot}5\,^\circ$C which, for the $Re = 15000$ case, corresponds to a Reynolds-number variation of ± 350. The volume flow rate was checked by integrating the velocity profile at each station and comparing with the reading taken from a rotameter-type flowmeter, whose accuracy had been found to be reliable by using the familiar technique of 'bucket and stop-watch'. In the constant-diameter sections of

the tube the maximum disagreement between the integrated velocity profile and the flowmeter reading was 8·7 %. At $Z = -1$, within the constriction segment of the stenosis, the disagreement had a value of 14·5 %.

Data analysis

A block diagram depicting the LDA and data acquisition system was given in figure 2. Ideally, the analog output of the phase-lock loop of the frequency tracker is related to the flow velocity through the Doppler equation

$$f_D = 2u \sin i/\lambda. \tag{1}$$

The electronics of the system are designed to remove the d.c. offset introduced by the Bragg cell. This output is averaged with an integrating voltmeter for a period of from 30 to 300 s, depending upon the degree of turbulence. The signal is also introduced into a 'Hewlett-Packard 5451A Fourier Analyzer' after low-pass filtering to prevent aliasing (Krohn-Hite Filter, Model 3342 R with 46 dB attenuation per octave). The Fourier analyser contains an analog-to-digital converter which, for the present study, digitized 1 s samples of data into 1024 discrete points, yielding a frequency resolution of 1 Hz and a maximum frequency of 512 Hz. These sampling parameters were selected after considerable experimentation. A discrete fast Fourier transform and complex-conjugate multiplication yielded the energy spectrum for a given sample. Averaging of 50 to 100 samples resulted in stable and repeatable spectra which were integrated, after subtracting the square of the mean velocity, to give the square of the disturbance velocity. A teleprinter and x, y plotter were used as output modes for the Fourier analyser.

Pressure measurement

Wall pressures were measured as a difference in water column height using a simple inclined tube manometer system with the reference port being located just prior to the constriction ($Z = -2{\cdot}5$).

3. Results

Preliminary studies

Initially, studies were performed at the station $Z = -4$, which is reasonably representative of fully developed pipe flow, at a Reynolds number $Re = 2\bar{u}a_0/\nu$, of $15\,000 \pm 350$, where $\bar{u}$ is the average flow velocity in the tube and ν is the kinematic viscosity. Volume flow rates obtained at this station by integrating the LDA measurements were consistently within 2 % of those given by the flowmeter. The turbulence fluctuations $u'_{\text{r.m.s.}}$ and $w'_{\text{r.m.s.}}$ obtained at $Z = -4$ and $Re = 15\,000$ are shown in figure 4 and they should correspond to fully developed pipe flow. Also presented are the curves from the experimental data of Laufer (1954) for fully developed flow at $Re = 40\,600$. It is possible to extrapolate his measurements to the present case of $Re = 15\,000$ in the following approximate manner. When the turbulence velocities $u'_{\text{r.m.s.}}$, $v'_{\text{r.m.s.}}$ and $w'_{\text{r.m.s.}}$ reported by Laufer are non-dimensionalized by friction velocity u^* and compared for two Reynolds numbers (40 000 and 418 500), they are seen to be independent of Re in the core region, $R \lesssim 0{\cdot}8$. If the Blasius formula (Schlichting 1968) relating the pressure gradient and Reynolds number in a fully developed turbulent pipe flow and

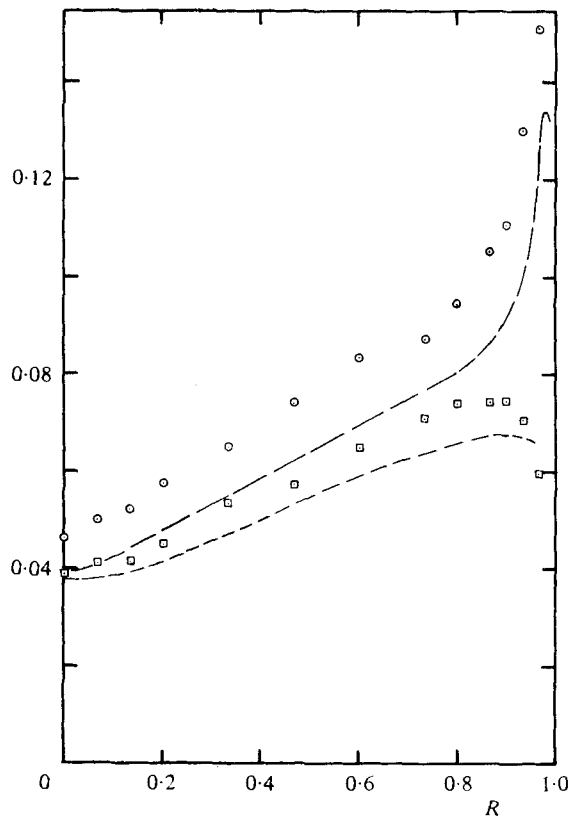

FIGURE 4. Turbulence velocity components measured upstream of the stenosis at $Re = 15000$, $Z = -4$: ⊙, $u'_{\text{r.m.s.}}/\bar{u}$; ⊡, $w'_{\text{r.m.s.}}/\bar{u}$. Laufer (1954), fully developed pipe flow $Re = 40600$; — —, $u'_{\text{r.m.s.}}/\bar{u}$; – – –, $w'_{\text{r.m.s.}}/\bar{u}$.

the fact that pressure gradient varies as u^{*2} are combined, it follows that turbulence velocity fluctuations, as non-dimensionalized by $\bar{u}$, at $Re = 15000$ should be approximately 13 % higher than the corresponding values at $Re = 40600$. The good comparison, though indirect, enhances the confidence in the measurement of $u'_{\text{r.m.s.}}$ and $w'_{\text{r.m.s.}}$ using the LDA system.

Flow reattachment

In a turbulent flow it is difficult to identify a reattachment point owing to the large fluctuations occurring. In the following discussion the reattachment 'point' is considered to be the position where the mean velocity gradient at the wall changes sign. The mean shear stress does not necessarily vanish at this point. The reattachment point was located by measuring the velocity close to the wall at several points 0·10 in. (0·25 cm) apart in the axial direction. By graphing the velocity at each point, the position at which the mean velocity changes sign could be found. Integration time for each velocity measurement varied from 45 to 500 s, with the longer duration being necessary close to the reattachment point. This was required due to high values of fluctuating velocity and integral time scale and due to a very small velocity magnitude. These experiments circumvent the difficulties involved in determining the reattach-

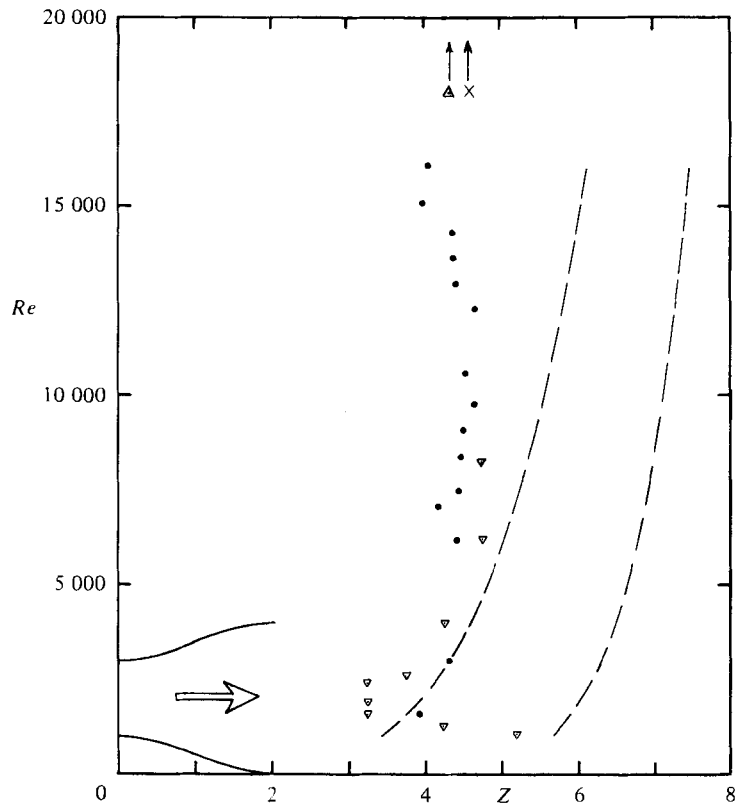

FIGURE 5. Location of reattachment for various Reynolds numbers: ▽, Roschke & Back (1976); — —, Clark (limits) (1976); ●, present results. High-Reynolds-number values; ×, Chaturvedi (1963); △, Teyssandier & Wilson (1974).

ment point in a turbulent flow using dye injection techniques and should provide a substantial improvement in accuracy over visual studies.

The results obtained for several Reynolds numbers are indicated in figure 5. Also shown are the results of Roschke & Back (1976) for the distance to reattachment following an abrupt expansion in a pipe. Although the geometries used are not exactly the same in the two cases, the results are in reasonable agreement for the Reynolds-number range of overlap. The reattachment location is not very sensitive to the Reynolds number in the range examined here although there is a slight, but noticeable, decrease for Reynolds numbers decreasing from 6000 and increasing from 13 000.

Flow velocities

Mean velocity profiles were measured at several stations from $Z = -4$ to 11 and for three Reynolds numbers: 5000, 10 000 and 15 000. The time-averaged axial velocity component $\langle u \rangle$ is shown non-dimensionalized by the bulk velocity $\bar{u}$ obtained by integrating the mean velocity profile at each location. The most detailed measurements were taken at $Re = 15\,000$ and these are presented in figure 6, which is separated into two parts for clarity. The velocity profile at $Z = -4$ is in reasonable agreement with the fully developed, power-law profile ($n \cong 6{\cdot}4$) for this Reynolds number. The measured

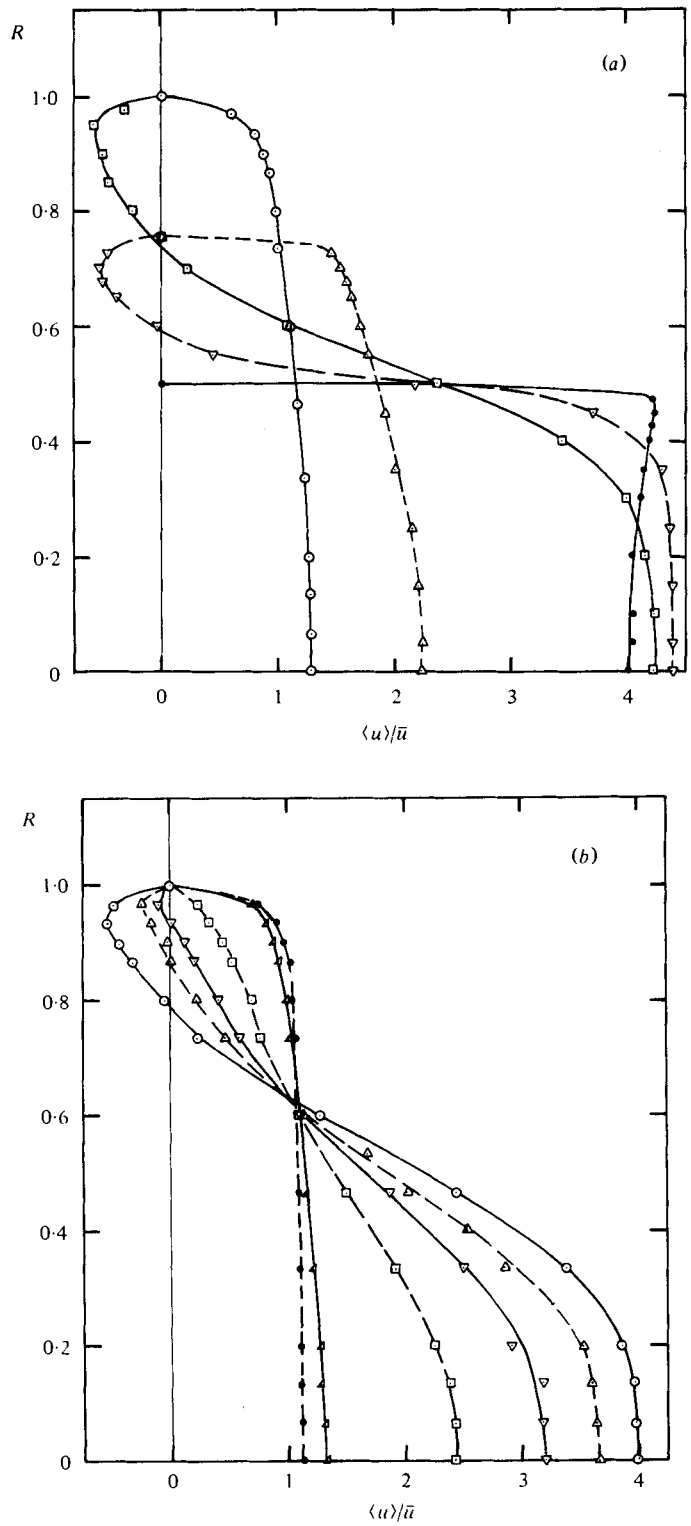

FIGURE 6. Axial velocity profiles, $Re = 15000$. (*a*) ○, $Z = -4$; △, $Z = -1$; ●, $Z = 0$; ▽, $Z = 1$; ⊡, $Z = 2$. (*b*) ○, $Z = 2{\cdot}5$; △, $Z = 3{\cdot}5$; ▽, $Z = 4$; ⊡, $Z = 5$; ◿, $Z = 8$; ●, $Z = 11$. Lines for visual aid only.

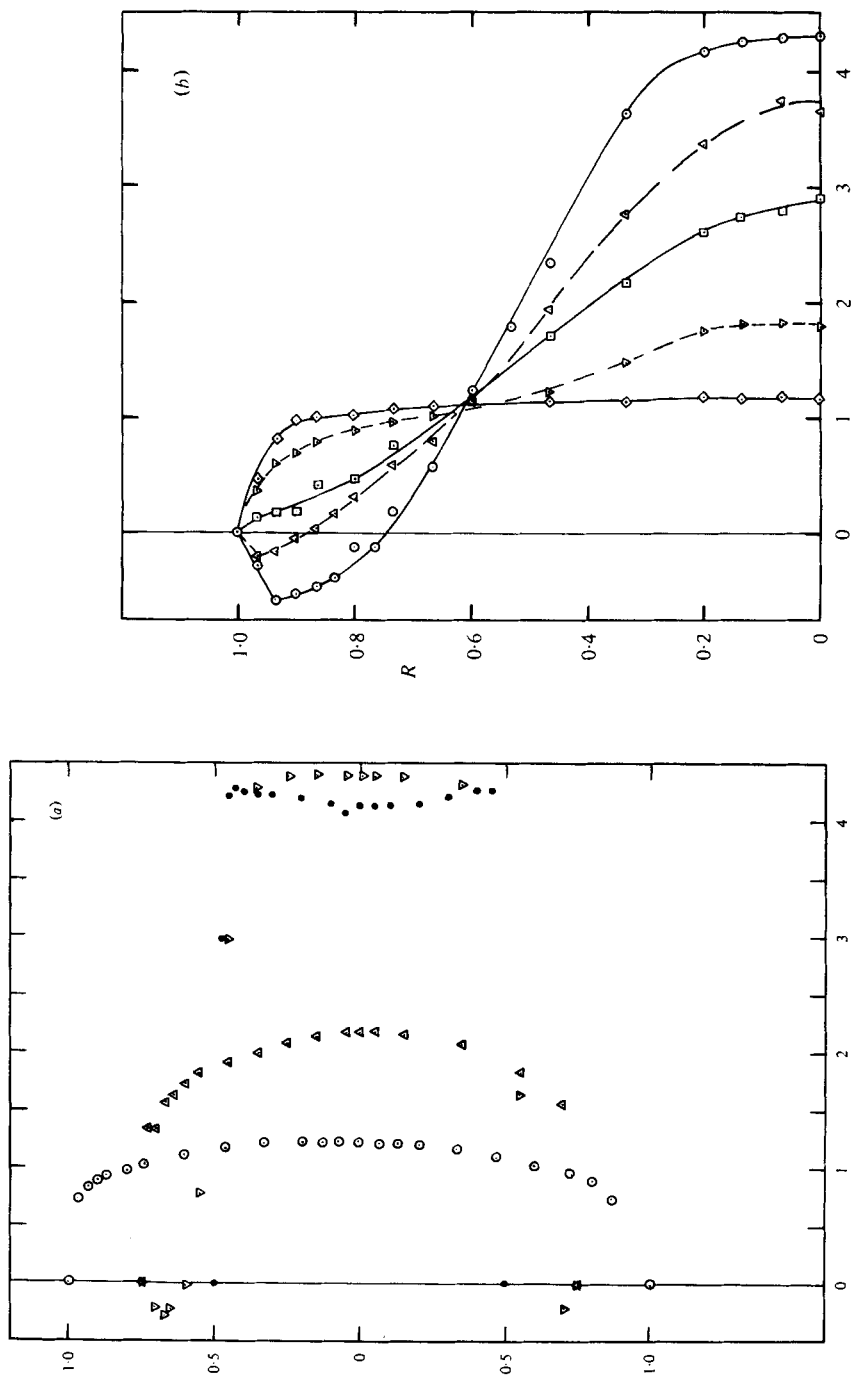

FIGURE 7. Axial velocity profiles, $Re = 10000$. (*a*) ○, $Z = -4$; △, $Z = -1$; ●, $Z = 0$; ▽, $Z = 1$. (*b*) ⊙, $Z = 2{\cdot}5$; △, $Z = 4$; ⊡, $Z = 5$; ▽, $Z = 7$; ◇, $Z = 11$. Lines for visual aid only.

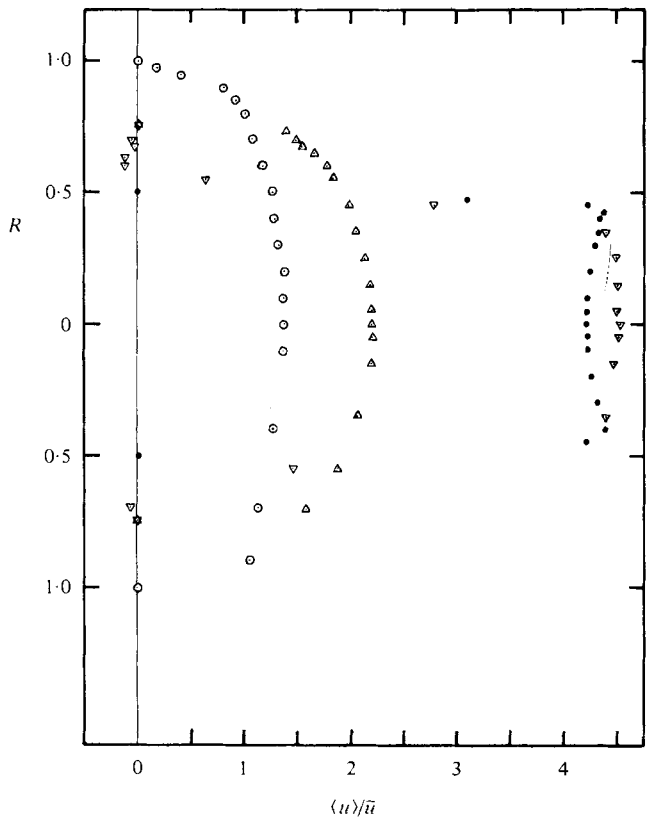

FIGURE 8. Axial velocity profiles, $Re = 5000$. ⊙, $Z = -2$; △, $Z = -1$; ●, $Z = 0$; ▽, $Z = 1$.

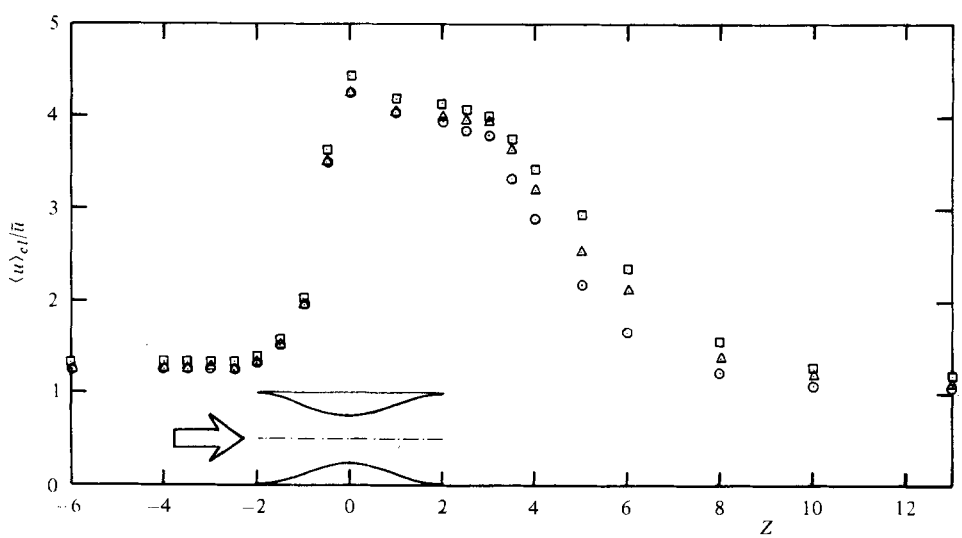

FIGURE 9. Axial variation of centre-line velocity for different Reynolds numbers. ⊡, $Re = 5000$; △, $Re = 10000$; ○, $Re = 15000$.

profile at the entrance plane of the constriction ($Z = -2$) was very close to that at $Z = -4$. A brisk acceleration in the converging section is demonstrated by the data points for $Z = -1$; and a rather blunt, plug-like profile is seen at the throat, $Z = 0$. Interestingly, the maximum velocity does not occur at the centre-line but occurs at a near-wall station. This phenomenon was predicted for several laminar flow computations by Deshpande *et al.* (1976) and for a two-equation model computation for turbulent flow by Deshpande (1977). Flow recirculation is distinctly apparent in the profiles from $Z = 1$–4. It can be noted that negative velocities as high as 60 % of the upstream bulk velocity occur in the region of separated flow. Flow reattaches, in a mean sense, just prior to $Z = 5$; and the profiles following this station reflect a gradual return toward the upstream condition. This return is not monotonic, however, in that the profile at $Z = 11$ is flatter than the upstream profile and, consequently, flatter than the relevant power-law shape. As will be seen in later figures, turbulence intensities at $Z = 11$ remain considerably greater than the fully developed pipe flow values.

Measured profiles for $Re = 10000$ are shown in figure 7 for a similar set of stations, and a smaller set of data for $Re = 5000$ are shown in figure 8. If the profiles for the various Reynolds numbers are graphed at corresponding stations, it is found that those for $Z \leqslant 0$ are remarkably similar. In the diverging section of the constriction, of course, such is not the case. The prestenotic flow field is thus considerably less sensitive to changes in Reynolds number than is the poststenotic field. Figure 9 illustrates the axial variation of the centre-line velocity. Again, it is seen that the velocity along the axis dips under the fully developed value, bearing an interesting similarity to the case of turbulent flow development in the entrance region of a pipe where the centre-line mean velocity reaches a maximum and then recedes to its final value as flow develops (e.g. Melling & Whitelaw 1976; Deshpande & Giddens 1978). Flows at the three Reynolds numbers differ substantially beyond the nozzle exit.

Wall pressure

The distribution of static pressure along the wall is given in figure 10. As expected, there is a steep decline of the pressure in the converging section as the flow is sharply accelerated. There is a brief rapid rise in the first half of the diverging section and then very little change until the flow passes through the exit plane of the stenosis. The major portion of the pressure recovery occurs distal to the constriction. A relative maximum is located near $Z = 8$ which, in contrast to laminar flow (Deshpande *et al.* 1976), is not particularly sensitive to the Reynolds number over the range studied. The Blasius formula for a smooth pipe (e.g. Schlichting 1968) is shown for comparison. The net pressure drop between $Z = -2{\cdot}5$ and 16 can be approximated very well by the relation

$$\frac{\Delta p}{\rho \bar{u}^2} = \frac{24{\cdot}5}{Re^{0{\cdot}174}}. \tag{2}$$

Turbulence velocity fluctuations

Turbulence velocities, $u'_{\text{r.m.s.}}$ and $w'_{\text{r.m.s.}}$ measured at several representative stations and at $Re = 15000$ are shown in figures 11 and 12 using the bulk velocity $\bar{u}$ upstream of the stenosis as a non-dimensionalizing parameter. Figure 11 (*a*) gives the $u'_{\text{r.m.s.}}$ and $w'_{\text{r.m.s.}}$ variations at $Z = -1$ while figure 11 (*b*) presents data from the $Z = 0$ location. Results at $Z = -4$ were given in figure 4. The longitudinal component is seen to attenuate

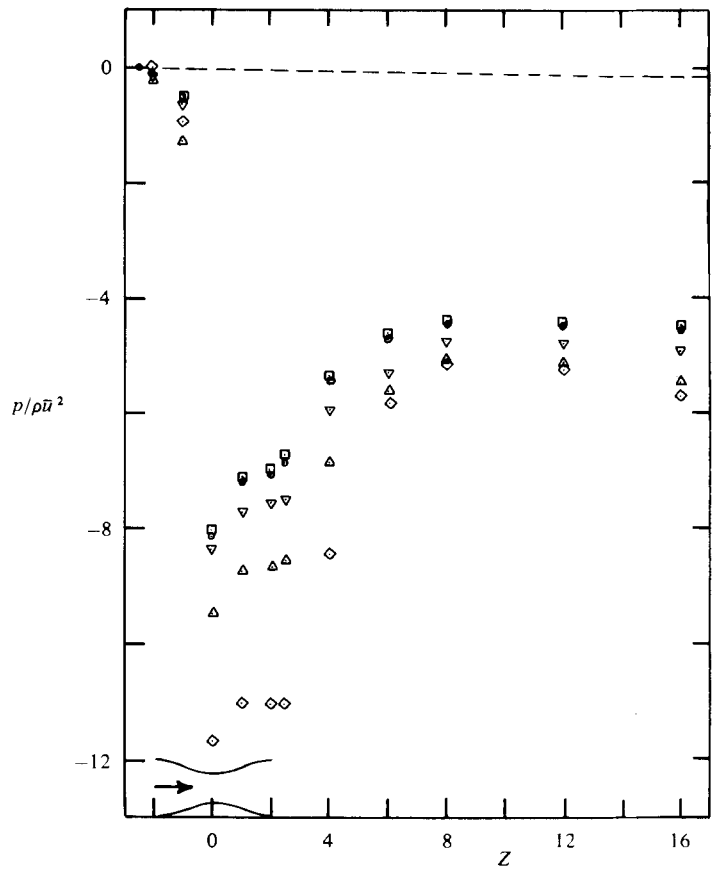

FIGURE 10. Distribution of non-dimensional wall pressure through the stenosis for different Reynolds numbers. ◇, Re = 4425; △, Re = 7500; ▽, Re = 10000; ○, Re = 15300; □, Re = 16260. – – –, smooth pipe, Re = 4425.

slightly in the converging section of the constriction while the azimuthal component is amplified. This is consistent, for example, with the data of Hussain & Ramjee (1976) for wind tunnel turbulence.

Sharp increases in $u'_{\text{r.m.s.}}$ and $w'_{\text{r.m.s.}}$ occur in the diverging section. Figures 12(*a*) and (*b*) present $u'_{\text{r.m.s.}}$ and $w'_{\text{r.m.s.}}$ at Z = 1, 2, 4, 6 and 11. The longitudinal component is greatly amplified in the shear-layer region at Z = 1. The largest fluctuation velocities occur, as expected, in the shear layer. It is not until downstream of reattachment that the centre-line fluctuations are the largest at a given station. Also, there is a very clearly non-isotropic turbulent behaviour in the poststenotic field with $u'_{\text{r.m.s.}}$ often being more than 50 % larger than $w'_{\text{r.m.s.}}$. Two-equation turbulence models will thus be hard pressed to give accurate flow predictions in this region. Measurements were made as far downstream as Z = 11 and, although mean velocity profiles were found to be approaching a fully developed state (figure 6), the turbulence velocities at Z = 11 were from two to five times greater than those at $Z = -4$.

Figure 13(*a*) gives the variation of $u'_{\text{r.m.s.}}/\bar{u}$ measured at the centre-line while figure 13(*b*) presents the axial variation of the maximum value of $u'_{\text{r.m.s.}}/\bar{u}$. The distinction between these curves in the near field of the poststenotic region is readily apparent.

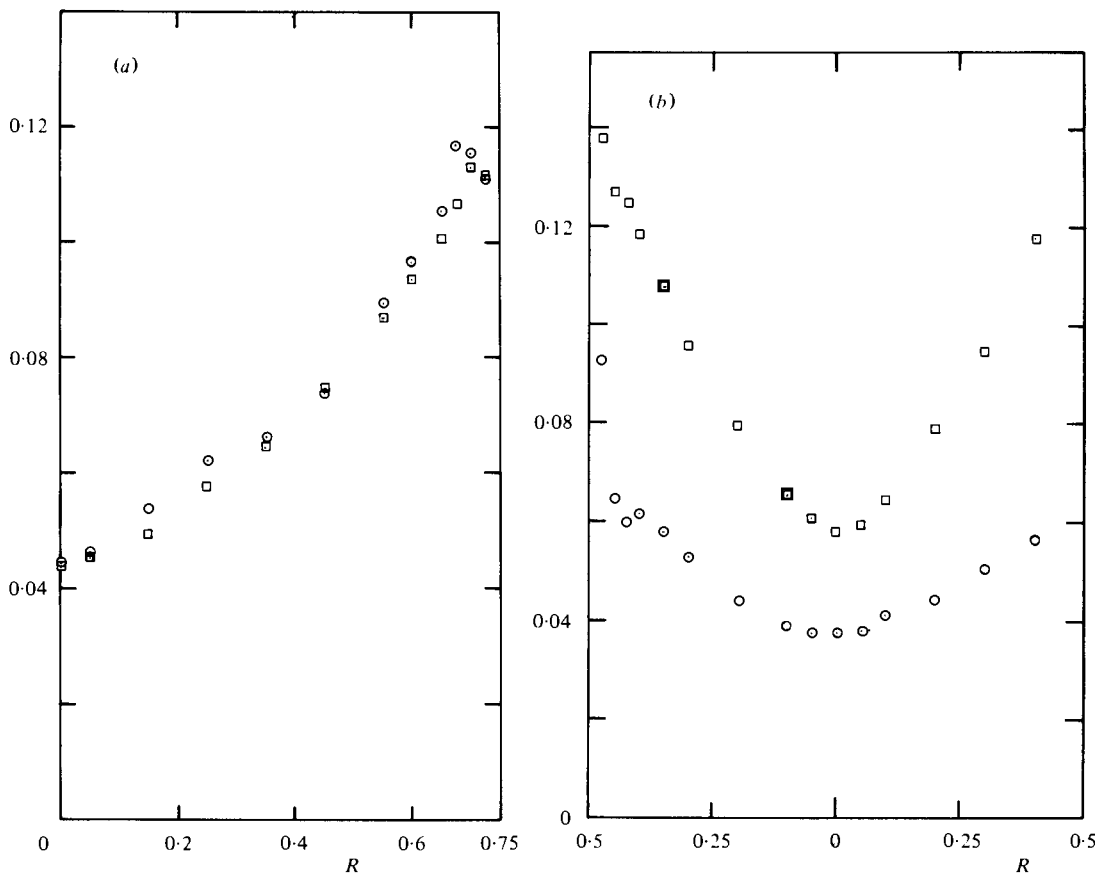

FIGURE 11. Profiles of turbulence velocity components at $Re = 15000$. (*a*) $Z = -1$: ⊙, $u'_{\text{r.m.s.}}/\bar{u}$; ⊡, $w'_{\text{r.m.s.}}/\bar{u}$. (*b*) $Z = 0$ (throat): ⊙, $u'_{\text{r.m.s.}}/\bar{u}$; ⊡, $w'_{\text{r.m.s.}}/\bar{u}$.

Energy spectra

The spectral function $E(f)$ is a measure of the energy content per unit frequency of the velocity signal. Energy spectra were computed from the measured data using 'Fast Fourier Transform' techniques on the HP 5451A Fourier analyser. It is convenient to employ the normalized spectrum

$$F(f) = \frac{E(f)}{u'^2_{\text{r.m.s.}}}$$

and the dimensionless variables

$$E^* = FU/2\pi l \quad \text{and} \quad N_S^* = 2\pi f l/U,$$

where $u'^2_{\text{r.m.s.}}$ is the mean-square velocity fluctuation, l is a characteristic length, and U is a characteristic velocity. The proper length and velocity scales are difficult to define in a poststenotic flow. For example, near the throat the constriction diameter and velocity are appropriate scaling parameters whereas this is not necessarily the case farther downstream, particularly after flow reattachment. The approach taken here will be to employ the constriction diameter as the length scale in regions between the throat and reattachment and the tube diameter elsewhere. Choice of the proper

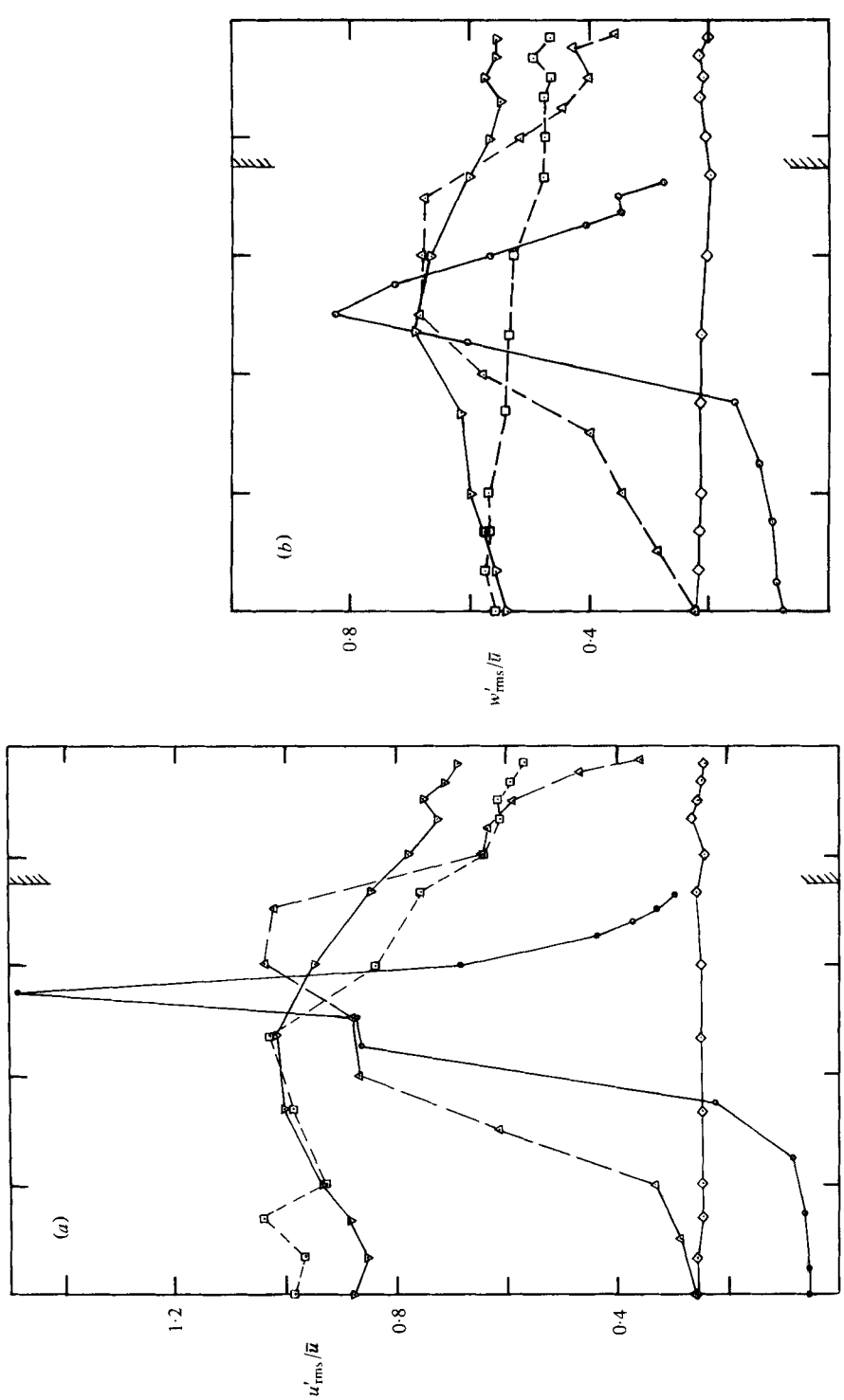

FIGURE 12. Profiles of turbulence velocity components at different axial locations, $Re = 15000$. (*a*) $u'_{\mathrm{r.m.s.}}/\bar{u}$: ⊙, $Z = 1$; △, $Z = 2$; ▽, $Z = 4$; □, $Z = 6$; ◇, $Z = 11$. (*b*) $w'_{\mathrm{r.m.s.}}/\bar{u}$: ⊙, $Z = 1$; △, $Z = 2$; ▽, $Z = 4$; □, $Z = 6$; ◇, $Z = 11$. Lines for visual aid only.

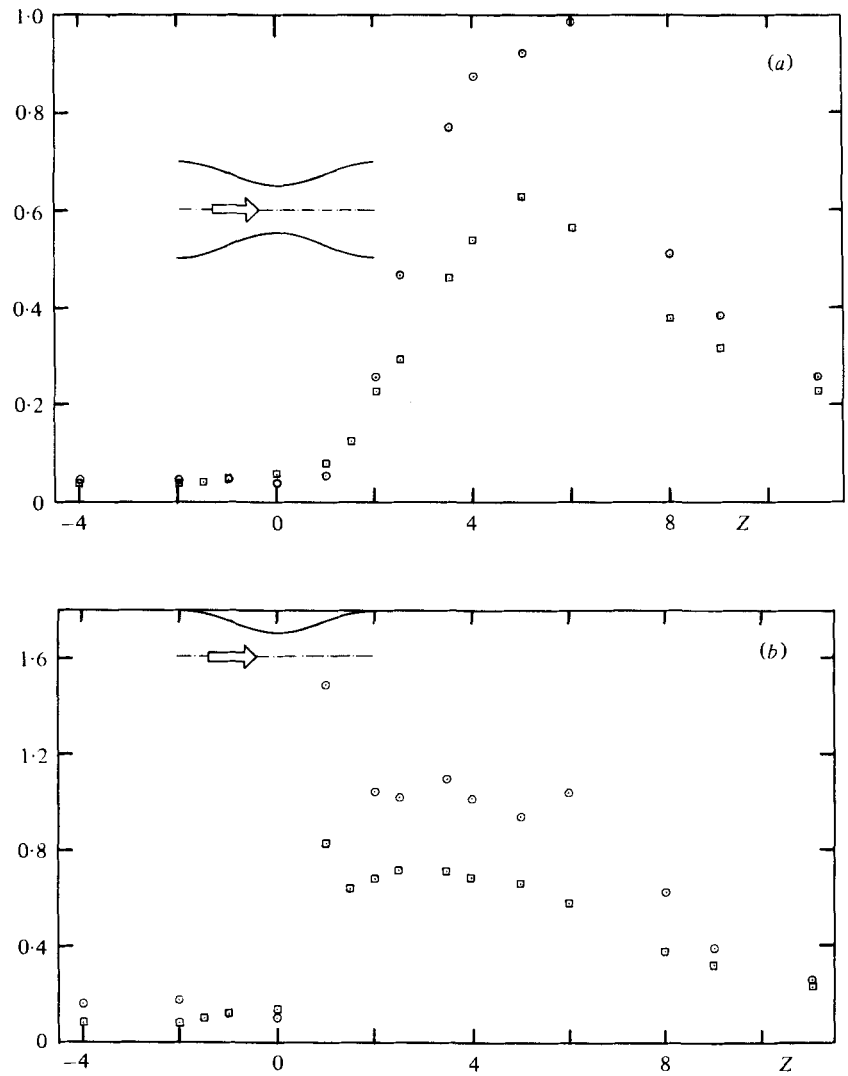

FIGURE 13. (*a*) Variation of the centre-line values of turbulence velocity fluctuations $u'_{\text{r.m.s.}}/\bar{u}$ and $w'_{\text{r.m.s.}}/\bar{u}$, $Re = 15\,000$. ⊙, $u'_{\text{r.m.s.}}/\bar{u}$; ⊡, $w'_{\text{r.m.s.}}/\bar{u}$. (*b*) Variation of the maximum values of turbulence velocity fluctuations $u'_{\text{r.m.s.}}/\bar{u}$ and $w'_{\text{r.m.s.}}/\bar{u}$, $Re = 15\,000$. ⊙, $u'_{\text{r.m.s.}}/\bar{u}$; ⊡, $w'_{\text{r.m.s.}}/\bar{u}$.

velocity scale is made difficult by the fact that the poststenotic field contains a wide range of velocities, including negative values within the recirculation region. The dimensionless spectra presented in this section were obtained using the centre-line velocity as the characteristic parameter.

Figure 14(*a*) gives results obtained at $Z = -4$ upstream of the constriction at $Re = 15\,000$. Data for the longitudinal velocity component at several radial stations are shown and compared with the hot-film measurements of Resch (1970) in a fully developed turbulent pipe flow at the same Reynolds number. Agreement between the present results and those of Resch is quite good except for the very high frequency segment of the curves, where noise and ambiguity become apparent in the laser results.

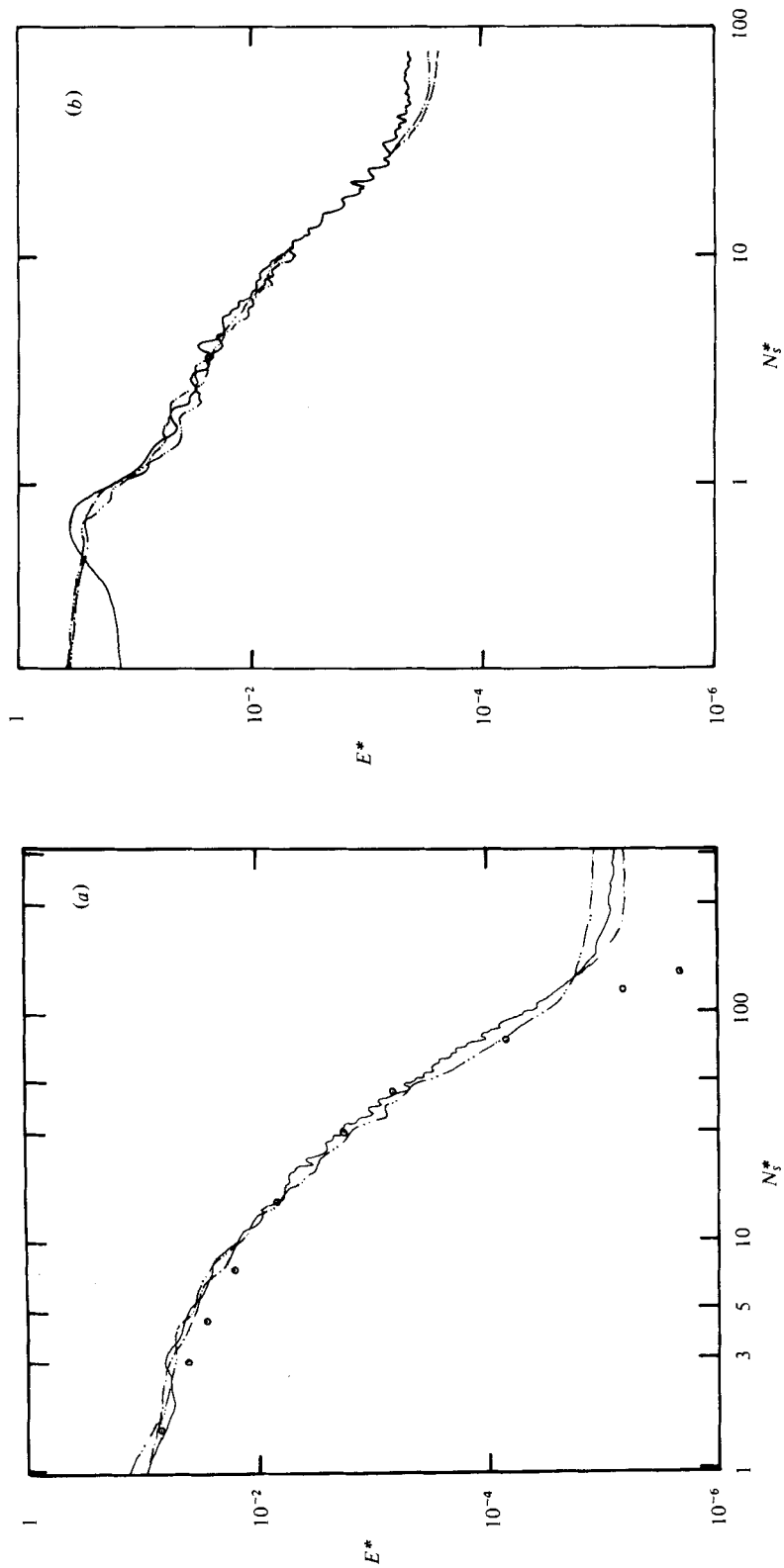

FIGURE 14. For legend see facing page.

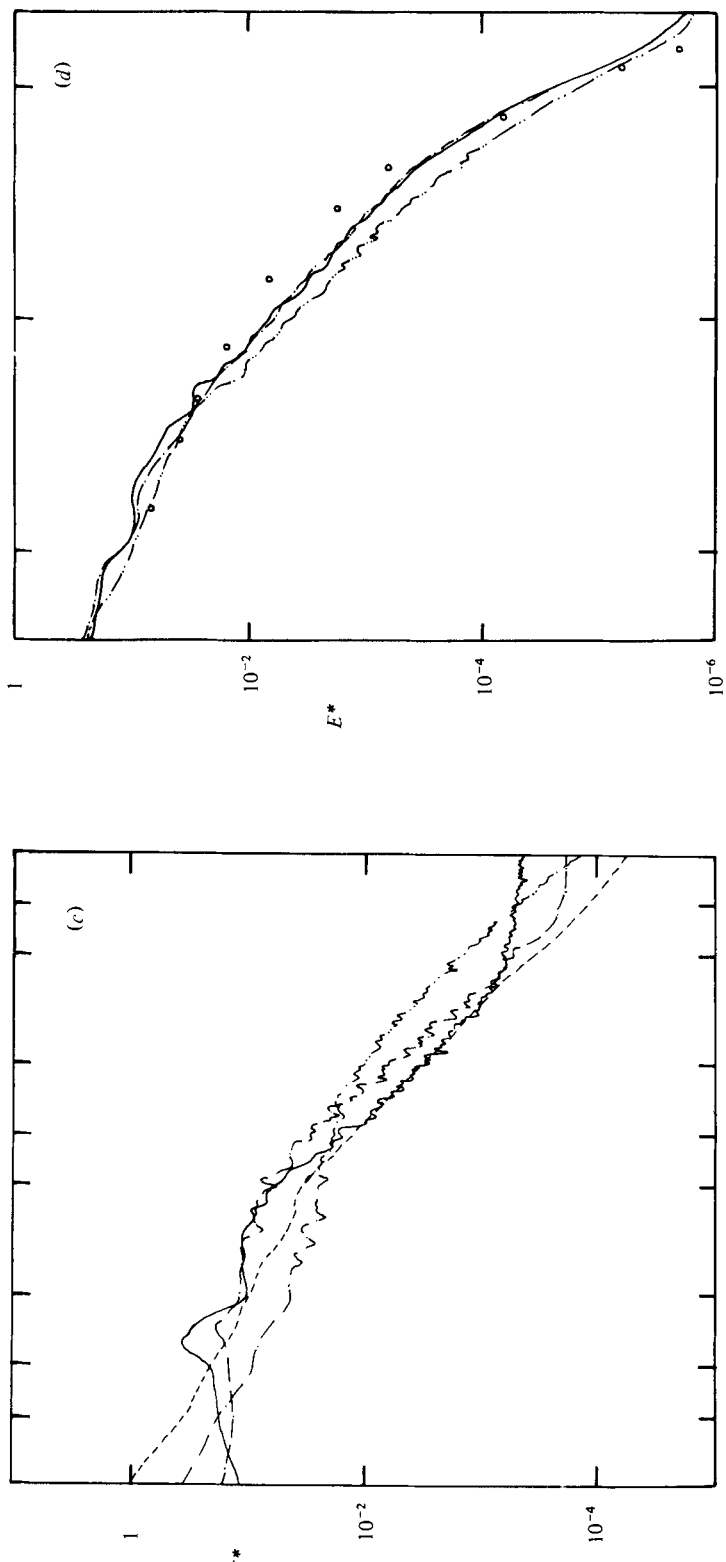

FIGURE 14. Energy spectra E^* for $u'_{r.m.s.}$ at $Re = 15000$. (*a*) $Z = -4$: ——, $R = 0{\cdot}333$; -·-, $R = 0{\cdot}60$; -··-, $R = 0{\cdot}933$; ○, Resch (1970) ($Re = 15000$, $D = 44$ mm, $R = 0{\cdot}0$). (*b*) $Z = 0$ (throat): ——, $R = 0{\cdot}0$; -·-, $R = 0{\cdot}30$; -··-, $R = 0{\cdot}45$. (*c*) $Z = 1{\cdot}0$: ——, $R = 0{\cdot}0$: - · -, $R = 0{\cdot}25$; -···-, $R = 0{\cdot}45$; – – –, $R = 0{\cdot}70$. (*d*) $Z = 4{\cdot}0$: ——, $R = 0$; -·-, $R = 0{\cdot}467$; -···-, $R = 0{\cdot}867$; ○, Resch (1970) ($Re = 15000$, $D = 44$ mm, $R = 0{\cdot}0$).

Figure 14 (*b*) shows measurement results obtained at the throat, taking the characteristic length to be the throat diameter. Again, spectra for the various radial stations are similar except for a low frequency peak at the centre-line station. This appears to be due to the influence of shed vortices. The peak occurs at approximately four hertz at both the $R = 0$ and $R = 0{\cdot}1$ stations for $Z = 0$ and, as seen in figure 14 (*c*), occurs at $R = 0$ for $Z = 1$. It is not readily apparent at other locations measured, due to the fact that breakup into turbulence has occurred. Even at stations that do demonstrate such peaks, however, the spectra show the coexistence of high frequency random fluctuations.

Spectral measurements at several radial stations for $Z = 1$ are shown in figure 14 (*c*). The characteristic length is taken to be the throat diameter in these non-dimensional co-ordinates. Although the raw data for the spectra become grouped much more closely when graphed using the non-dimensional variables, the good similarity among various radial stations which was seen at upstream locations does not occur in this extremely turbulent region. Identification of the remnants of shed vortices is very difficult except in the centre-line spectrum.

At $Z = 4$ the radial spectra are again similar to each other (figure 14*d*) although they are not similar to turbulent pipe-flow data. Since reattachment occurs near this station, the characteristic length is taken to be D. No trace periodic vortex shedding can be seen in the data. It is perhaps noteworthy that employment of the centre-line velocity as a characteristic parameter scales the spectra so well, since the average velocity varies from approximately 80 cm s^{-1} at the centre-line to very nearly zero at $R = 0{\cdot}867$ (refer to figure 6 (*b*) which shows that $Z = 4$ is very near the reattachment station and the mean velocity values are quite low for $R > 0{\cdot}8$). Resch's data for $Re = 15\,000$ are again shown for comparison and it is seen that the present spectra, although radially similar, have not yet recovered to a characteristic pipe flow spectral shape.

Figure 15 gives a comparison of centre-line spectra taken under a variety of conditions. The present LDA measurements are shown for $Z = 4$, 6 and 11 downstream of the 75 % constriction. Resch's pipe flow measurements at $Re = 15\,000$ are also placed on the graph, along with a curve taken from Clark's hot-film studies on turbulence distal to stenoses. Khalifa & Giddens (1978) have reported on *in vivo* measurements with hot films distal to stenoses imposed on the dog aorta, covering a range of constrictions from 25 to 88 % and at a peak Reynolds number in the unoccluded aorta of approximately 2000. Extraction of turbulence fluctuations during the deceleration phase of the pulsatile velocity waveforms led to a set of data as shown in figure 15 (see figure 6 (*b*) of Khalifa & Giddens). The deceleration phase of the waveforms was selected for comparison since this was the period of greatest flow instability for these *in vivo* data at relatively low Reynolds number. The characteristic length was taken to be the constriction diameter since the measurements were made very close to the stenosis. Examination of figure 15 shows that there is a fair correlation of the turbulence measurements taken over a wide variety of flow conditions.

4. Discussion

The method employed here using the laser-Doppler anemometer should provide a far superior technique for locating the reattachment 'point' than visual methods. The large velocity fluctuations in the neighbourhood of reattachment would quickly

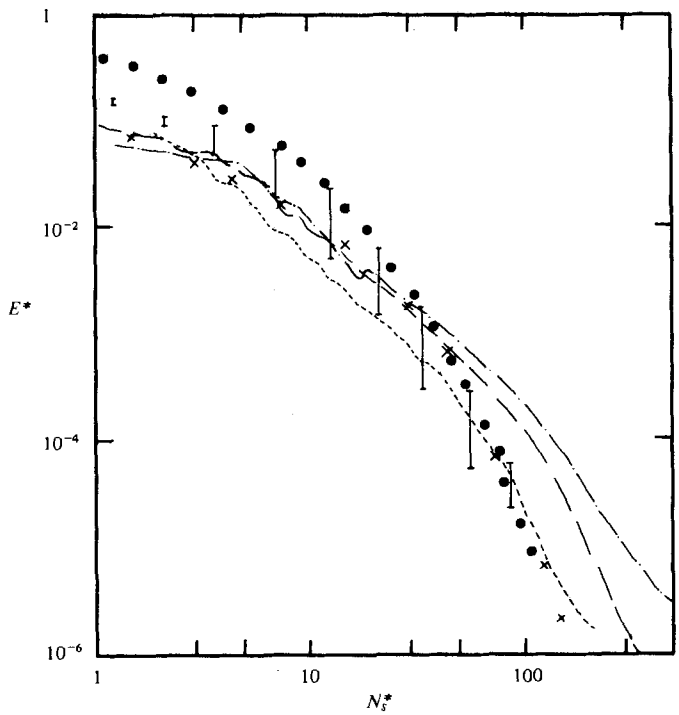

FIGURE 15. Energy spectra E^*. ●, Clark (1976); ×, Resch (1970);], Khalifa & Giddens (1978). Present study at $R = 0$: – – –, $Z = 4$; — —, $Z = 6$; –·– $Z = 11$.

diffuse a dye, obliterating vision. More fundamentally, however, is the fact that specifying a point of reattachment requires a very long averaging time since the entire region is in considerable turmoil. Sufficiently long observations with flow visualization methods are extremely difficult. The present data show that the length of the circulation region is almost constant with Reynolds number over the range studied. In fact, there is a slight tendency for this length to decrease at the higher Reynolds numbers. This is different from the behaviour reported by Clark (1976) using flow visualization. Clark used a dye-injection method to determine the upstream and downstream limits of which he termed a 'reattachment zone', i.e. distal to several nozzles of various geometries. The empirical relations proposed in that reference are shown in figure 5. The present data fall within these limits at the lower Reynolds numbers, but the trend with increasing Reynolds number is not in agreement with Clark's relations. We can think of two possible reasons for this discrepancy. First, Clark's geometries are somewhat different from the one employed in the present study in that the constriction segment of the stenosis was tapered from the inlet to a 'short parallel length of the required final cross-section'. The expansion then occurred abruptly. As discussed in §1, the dynamics of the recirculation region will depend to some degree upon the conditions prevailing upstream of separation. For example, Hussain & Zedan (1978) report on the effects of the initial boundary layer upon a free-shear-layer development. However, despite this sensitivity we speculate that the contrast between Clark's data and ours cannot be accounted for solely on this basis, since conflicting trends with increasing Reynolds number occur. To support this speculation we indicate in figure 5

the high-Reynolds-number reattachment points measured by Chaturvedi (1963) and calculated by Teyssandier & Wilson (1974). These values are $Z = 4{\cdot}6$ and $4{\cdot}36$, respectively, for the case of a sudden expansion in a pipe with upstream to downstream area ratio of $0{\cdot}25$, which corresponds to a stenosis area reduction of 75 %. Chaturvedi's data point comes from studies at a throat Reynolds number of 2×10^5 while the analysis of Teyssandier & Wilson, although not specifying a particular Reynolds number, assumes an asymptotically 'high' value. Thus, there is evidence that a continual increase in reattachment length with Re does not occur.

A more likely explanation for the differences in the present data and that of Clark is the method for detecting reattachment. Dye injection methods depend upon visual inspection and, when employed in a highly turbulent flow, must be extremely difficult to interpret. The near-wall measurements with the laser, on the other hand, do not suffer from uncertainties, provided one has the patience to allow the time-averaged velocity to reach a steady value.

The centre-line velocity variation with axial position is consistent with the observation of the reattachment point. There is very little influence of Reynolds number upon the centre-line velocity until after reattachment has occurred. Another feature shown in the present data is the negative mean velocity found in the recirculation region. The LDA performed admirably in measuring this, and it was found that negative velocities of relatively large magnitude were present. This fact, coupled with the high values of velocity fluctuations occurring, would suggest that wall shear stresses in the separated zone could be higher than might be expected.

The rapid distortion theory by Batchelor & Proudman and by Ribner & Tucker (see Hussain & Ramjee 1976) when applied to the convergent portion of the nozzle with 75 % area reduction suggests a 54 % decrease in $u'_{\text{r.m.s.}}$ and 74 % increase in $w'_{\text{r.m.s.}}$. The present experiments indicate that the above theory overpredicts both the attenuation of $u'_{\text{r.m.s.}}$ and amplification of $w'_{\text{r.m.s.}}$ in the present case, especially close to the axis. Beyond $Z = 1$, the value of $w'_{\text{r.m.s.}}$ was seen to be smaller than $u'_{\text{r.m.s.}}$. This is due to the mean kinetic energy being siphoned primarily into $u'_{\text{r.m.s.}}$, and later redistributed into $v'_{\text{r.m.s.}}$ and $w'_{\text{r.m.s.}}$.

Clark reports that the maximum value of $u'_{\text{r.m.s.}}$ occurred on the axis in cases of axisymmetric nozzles and that $u'_{\text{r.m.s.}}/\bar{u}$ (throat) was constant when the throat Reynolds number was increased beyond 9000. Highest value quoted in that reference for the 75 % nozzle was $u'_{\text{r.m.s.}}/\bar{u} \cong 0{\cdot}63$. A lower value of $(u'_{\text{r.m.s.}}/\bar{u})_{\max}$ at smaller Reynolds numbers for this nozzle was attributed to frequencies less than 22·5 Hz being excluded. The values measured in the present study, however, are considerably larger with the maximum occurring in the shear layer rather than on the axis. These were

$$(u'_{\text{r.m.s.}}/\bar{u})_{\max} = 1{\cdot}48 \quad \text{and} \quad (w'_{\text{r.m.s.}}/\bar{u})_{\max} = 0{\cdot}82,$$

found at the $Z = 1$ station. The maximum value measured by Chaturvedi (1963) for a 75 % nozzle and Re at the throat of 2×10^5 was $(u'_{\text{r.m.s.}}/\bar{u}) \cong 0{\cdot}8$. As mentioned earlier, the large differences between the values of Clark and the present data may be attributed to variations in the geometry and the methods of measurement; i.e. frequencies below 22·5 Hz were excluded by Clark and the fact that a simple hot-film probe is unable to measure reverse velocity (which was found to occur instantaneously even on the axis at certain locations) and also measures a weighted average of all three components of velocity. The maximum values measured on the axis in the present study were

$u'_{\text{r.m.s.}}/\bar{u} = 0{\cdot}99$ at $Z = 6$, and $w'_{\text{r.m.s.}}/\bar{u} = 0{\cdot}62$ at $Z = 5$. The position for this maximum in the measurements of Clark was at $Z = 6{\cdot}6$.

A comparison with the *in vivo* studies reported by Khalifa & Giddens (1978) is not straightforward since, owing to restrictions in probe placement in the dog aorta, a position of maximum intensity was not mapped in those measurements. However, it is possible to compare the ratio $u'_{\text{r.m.s.}}/\bar{u}_{\mathbb{Q}}$, where $\bar{u}_{\mathbb{Q}}$ is the locally measured centreline velocity. For the data reported by Khalifa & Giddens with a 74 % occlusion and employing the disturbance velocity measured during peak turbulence of the heart cycle at a point $Z = 3{\cdot}3$, this value is 0·40 and corresponds to an upstream Reynolds number of approximately 2000, based on peak velocity. The present data give a value of 0·50 at a similar station. The non-dimensionalized spectra obtained from *in vivo* studies by Khalifa & Giddens are in fair agreement with the present data, although there is clearly a somewhat different slope in the two sets of spectral data which may be due to differences of Reynolds number.

The peaks in the $u'^2_{\text{r.m.s.}}$ spectra at $Z = 0$ and $Z = 1$ may be attributed to vortex shedding. For flows through a confined orifice vortices may be shed corresponding to a free jet criterion (for small d/D), to a wall protuberance criterion (for d/D close to unity), or to some behaviour between these extremes. The peaks in the $u'^2_{\text{r.m.s.}}$ spectra occurring at approximately 4 Hz give a value $fd/\bar{u}_0$ of approximately 0·1, which is too low for a free jet behaviour (e.g. Clark 1976; Beavers & Wilson 1970; Becker & Massaro 1968).

Peak Reynolds numbers in the normal human aorta are in the range 5000–12 000 (McDonald 1960). Stein & Sabbah (1976) have performed hot-film measurements in humans with normal and stenosed aortas and in one case with a prosthetic valve. The turbulence fluctuations in the normal subjects were considerably lower than those in the pathologic cases. We cannot compare our results with those of that study, however, since Stein & Sabbah filtered out frequencies below 30 Hz and did not give data on the degree of stenosis.

The very high turbulence intensities in the shear layer and the greatly disturbed recirculation region, as described by laser-Doppler measurements in the present experiments, present a picture of extreme disorder in the poststenotic flow field. This may lead to red cell damage and thrombus formation (Smith *et al.* 1972; Stein & Sabbah 1974). Further, the large spatial extent of these disturbances should provide an easy target for noninvasive identification with Doppler ultrasound, provided the site is accessible via acoustic beam. Additional studies at lower Reynolds numbers and employing bifurcation models would be useful in the study of vascular disease of arteries such as the carotid and femoral.

The flowfield of a stenotic model has thus been probed non-invasively with the laser-Doppler anemometer and measurements have been presented which would not have been possible with the hot-film anemometer. The results are generally in qualitative agreement with hot-film results published previously on similar geometries; however there are quantitative differences. Although the present study was motivated by a biological situation, we have attempted to report flow field measurements in sufficient detail that the results will be useful to investigators interested in turbulence modelling and computational fluid dynamics. In fact, the latter motivation was one reason for performing the extensive turbulence velocity and spectral measurements at the Reynolds number of 15 000 which is somewhat above values to be expected in the circulatory system.

Appendix

Several sources of error exist in laser-Doppler anemometry and are discussed admirably by George & Lumley (1973). We briefly describe two factors relevant to our particular measurements.

A 1. *Doppler ambiguity*

The error incurred owing to Doppler ambiguity was estimated in the following manner, taking $Re = 15\,000$ as a specific example. The ambiguity level of the measured turbulence spectra was less than $10^{-4}\,\mathrm{cm^2\,s^{-2}\,Hz^{-1}}$. The integration of the spectra to obtain turbulence velocity was carried out from 0 to 512 Hz. Following George & Lumley, the estimated contribution of ambiguity to the mean-square turbulence velocity is then $512 \times 10^{-4}\,\mathrm{cm^2\,s^{-2}}$ and hence the estimate for the r.m.s. value is approximately $0{\cdot}2\,\mathrm{cm\,s^{-1}}$. For the value of $\bar{u}$ employed in creating the $Re = 15\,000$ flow this results in a contribution of 0·01 to the turbulence intensity $u'_{\mathrm{r.m.s.}}/\bar{u}$. It can be seen that this effect is much greater, percentage-wise, at the lower-intensity locations ($Z < 0$), but in all cases is on the order of 10 % or less.

A 2. *Truncation of the energy spectrum*

The error in the r.m.s. velocity due to truncation of the integral of the energy spectrum at 512 Hz can be estimated as follows. The non-dimensional graphs of the spectra in E^* and N_S^* co-ordinates indicate an approximate similarity with the data of Resch (1970). If the 'worst' case in the present data – that is the measurement location at which the energy spectrum at 512 Hz has the highest value (for u'^2 this occurs at $Z = 1$, $R = 0{\cdot}45$) – is taken as an example and is extrapolated following Resch's curve to the point where the power level reaches the ambiguity level ($10^{-4}\,\mathrm{cm^2\,s^{-2}\,Hz^{-1}}$), integration of the additional segment gives a contribution of about $1{\cdot}6\,\mathrm{cm\,s^{-1}}$ to the r.m.s. turbulence velocity. This is on the order of 10 % of the r.m.s. value found by integration of the spectrum to 512 Hz.

This research was supported by the National Science Foundation under Grant ENG74-21986 and by the National Institutes of Health under Grant HL15519.

REFERENCES

Beavers, G. S. & Wilson, T. A. 1970 Vortex growth in jets. *J. Fluid Mech.* **44**, 97.

Becker, H. A. & Massaro, T. A. 1968 Vortex evolution in a round jet. *J. Fluid Mech.* **31**, 435.

Chaturvedi, M. C. 1963 Flow characteristics of axisymmetric expansions. *Proc. A.S.C.E., J. Hydraul. Div.* **89**, 61.

Cherdron, W., Durst, F. & Whitelaw, J. H. 1978 Asymmetric flows and instabilities in symmetric ducts with sudden expansions. *J. Fluid Mech.* **84**, 13.

Clark, C. 1976 Turbulent velocity measurements in a model of aortic stenosis. *J. Biomech.* **9**, 677.

Deshpande, M. D. 1977 Steady laminar and turbulent flow through vascular stenosis models. Ph.D. thesis, Georgia Institute of Technology.

Deshpande, M. D. & Giddens, D. P. 1978 Turbulent entrance flow using a two-equation model. *Phys. Fluids* **21**, 510.

Deshpande, M. D., Giddens, D. P. & Mabon, R. F. 1976 Steady laminar flow through modelled vascular stenoses. *J. Biomech.* **9**, 165.

DURST, F., MELLING, A. & WHITELAW, J. H. 1974 Low Reynolds number flow over a plane symmetric sudden expansion. *J. Fluid Mech.* **64**, 111.

ETHERIDGE, D W. & KEMP, P. H. 1978 Measurements of turbulent flow downstream of a rearward-facing step. *J. Fluid Mech.* **86**, 545.

GEORGE, W. K. & LUMLEY, J. L. 1973 The laser-Doppler velocimeter and its application to the measurement of turbulence. *J. Fluid Mech.* **60**, 321.

GIDDENS, D. P., MABON, R. F. & CASSANOVA, R. A. 1976 Measurements of disordered flows distal to subtotal vascular stenoses in the thoracic aortas of dogs. *Circulation Res.* **39**, 112.

HUSSAIN, A. K. M. F. & RAMJEE, V. 1976 Effects of the axisymmetric contraction shape on incompressible turbulent flow. *J. Fluids Engng* **98**, 58.

HUSSAIN, A. K. M. F. & ZEDAN, M. F. 1978 Effects of the initial condition on the axisymmetric free shear layer: Effect of the initial fluctuation level. *Phys. Fluids* **21**, 1475.

KHALIFA, A. M. A. & GIDDENS, D. P. 1978 Analysis of disorder in pulsatile flows with applica- to poststenotic blood velocity measurement in dogs. *J. Biomech.* **11**, 129.

LAUFER, J. 1954 The structure of turbulence in fully developed pipe flow. *N.A.C.A. Rep.* 1174.

LEE, J. S. & FUNG, Y. C. 1970 Flow in locally constricted tubes at low Reynolds numbers. *J. Appl. Mech.* **37**, 9.

MCDONALD, D. A. 1960 *Blocd Flow in Arteries*, p. 53. London: Edward Arnold.

MELLING, A. & WHITELAW, J. H. 1976 Turbulent flow in a rectangular duct. *J. Fluid Mech.* **78**, 289.

NEREM, R. M. & SEED, W. A. 1972 An *in vivo* study of aorta flow disturbances. *Cardiovasc. Res.* **6**, 1.

RESCH, F. J. 1970 Hot-film turbulence measurements in water flow. *Proc. A.S.C.E., J. Hydraul. Div.* **96**, 787.

ROSCHKE, E. J. & BACK, L. H. 1976 The influence of upstream conditions on flow reattachment lengths downstream of an abrupt circular channel expansion. *J. Biomech.* **9**, 481.

SCHLICHTING, H. 1968 *Boundary Layer Theory*, 6th edn, p. 561. McGraw-Hill.

SEED, W. A. & WOOD, N. B. 1971 Velocity patterns in the aorta. *Cardiovasc. Res.* **5**, 319.

SIMPSON, R. L., STRICKLAND, J. H. & BARR, P. W. 1977 Features of a separating turbulent boundary layer in the vicinity of separation. *J. Fluid Mech.* **79**, 553.

SMITH, F. T. 1976 On entry-flow effects in bifurcating, blocked or constricted tubes. *J. Fluid Mech.* **78**, 709.

SMITH, R. L., BLICK, E. F., COALSON, J. & STEIN, P. H. 1972 Thrombus production by turbulence. *J. Appl. Physiol.* **32**, 261.

STEIN, P. D. & SABBAH, H. N. 1974 Measured turbulence and its effect upon thrombus formation. *Circulation Res.* **35**, 608.

STEIN, P. D. & SABBAH, H. N. 1976 Turbulent blood flow in the ascending aorta of humans with normal and diseased aortic valves. *Circulation Res.* **39**, 58.

TEYSSANDIER, R. G. & WILSON, M. P. 1974 An analysis of flow through sudden enlargements in pipes. *J. Fluid Mech.* **64**, 85.

YOUNG, D. F. & TSAI, F. Y. 1973 Flow characteristics in models of arterial stenosis I and II. *J. Biomech.* **6**, 395 and 547.